JOURNAL OF SOLID STATE CHEMISTRY 42, 191–205 (1982)

The Phase Diagram and Electrical Characteristics of Silver Iodo-Phosphate Fast-Ion Electrolytes

M. SAYER, S. L. SEGEL, J. NOAD, J. COREY, AND T. BOYLE

Department of Physics, Queen's University, Kingston, Ontario K7L 3N6, Canada

AND R. D. HEYDING

Department of Chemistry, Queen's University, Kingston, Ontario K7L 3N6, Canada

AND A. MANSINGH

Department of Physics and Astrophysics, Delhi University, Delhi, India

Received September 25, 1981

The equilibrium phase diagram for the $AgI/Ag_4P_2O_7$ system of fast-ion electrolyes is established along with the conductivity–composition relationship for polycrystalline samples. The highest conductivity compound (0.07 Ω^{-1} cm^{-1} at 300 K) has the composition $Ag_{16}I_{12}P_2O_7$. Measurements of relative permittivity and conductivity over a frequency range of 50 Hz to 100 kHz and a temperature range of 77 to 320 K on polycrystalline samples and single crystals of $Ag_{16}I_{12}P_2O_7$ show that the conductivity and its temperature dependence is anisotropic, with a higher conductivity along the c axis and a change in the activation energy for conduction from 0.4 eV at low temperatures to 0.14 eV above 300 K. Perpendicular to the c axis the activation energy is constant with temperature (0.28 eV). This anisotropy and a frequency dispersion in the ac conductivity between 110 to 150 K is shown to originate in the crystal structure of the material and in the distribution of Ag^+ ions between different sites.

1. Introduction

Fast-ion electrolytes in the silver iodide–silver oxyacid salt systems have been of interest in that they show high ionic conductivity at room temperature (*1*). The phase relationships in the system $AgI/Ag_4P_2O_7$ have been studied by Takahashi *et al.* (*2*). Four compounds are reported with nominal compositions $Ag_{19}I_{15}P_2O_7$ ($15AgI \cdot Ag_4P_2O_7$), $Ag_{16}I_{12}P_2O_7$ ($12AgI \cdot Ag_4P_2O_7$), $Ag_6I_2P_2O_7$ ($2AgI \cdot Ag_4P_2O_7$), and $Ag_9IP_4O_{14}$ ($AgI \cdot 2Ag_4P_2O_7$). The iodide-rich phases exhibit high silver ion conductivities (0.09 ohm^{-1} cm^{-1} at 300 K) with an activation energy of 0.14 eV between 293 and 420 K. The compounds are relatively stable and resistant to moisture, and Arora and Childs (*3, 4*) have recognized these properties for the fabrication of thin-film devices by vacuum evaporation. Similar systems have been investigated in a vitreous form (*5*). Quenched melts of mixtures of AgI with Ag_2SeO_4, $Ag_2Mo_2O_7$, etc., form glasses with high electrical conductivity, and glasses were obtained in the $AgI–Ag_2O–$

0022-4596/82/050191-15$02.00/0

P_2O_5 system by Minami *et al.* (*6*). The origin of such high conductivities in vitreous systems is still not well understood, and the phenomenon raises questions regarding the relative importance of long-range or short-range order in these types of fast-ion electrolytes.

A number of features of the electrical properties of AgI/Ag oxyacid salts are common to both vitreous and polycrystalline systems. These include a conductivity activation energy which becomes smaller at high temperatures (*5, 7*) and a frequency dispersion in the dielectric properties at frequencies below 100 kHz at temperatures between 100 and 150 K. Interpretation of the origin of these effects has been limited in many cases by the complexity of the systems concerned, a lack of large single crystals, and by experimental difficulties in analyzing electrical data on glasses and polycrystalline compacts.

In this work we have made a detailed study of the phase diagram of the $AgI/Ag_4P_2O_7$ system in order to establish the electrical properties of the single-phase compounds and to understand the effects of mixed phases in measurements on polycrystalline compacts. Following this work, single crystals of the compound with the highest conductivity (12 AgI; $Ag_4P_2O_7$) were grown by Garrett *et al.* (*8*) and the crystal structure was deduced. The conductivity is anisotropic with a temperature dependence which is also dependent on the orientation of the crystal. Below 100 K, the dielectric response has a frequency dispersion over the frequency range 50 Hz–100 kHz, which is characteristic of the bulk material and which originates in the distribution of ions over sites having different local energies. This is most clearly shown using electric modulus spectroscopy (*9*). The crystal structure and general properties of the system are found to be analogous to those of pyridinium silver iodide $(C_5H_5NH)Ag_5I_6$ (*10*).

2. Experimental

2.1. Sample Preparation and Characterization

(*a*) *Polycrystalline compacts.* Samples were prepared by mixing AgI and $Ag_4P_2O_7$ obtained from various sources in a ball mill or agate mortar and heating the mixtures in evacuated ($\leqslant$0.005 Torr) Pyrex ampoules to temperatures of 500–700 K. The specimens were subsequently annealed at 400–430 K for periods of 7–14 days, and were then cooled slowly to room temperature or quenched in liquid nitrogen. Attempts to form the silver iodopyrophosphate compounds at low temperatures by coprecipitation of I^- and $P_2O_7^{4-}$ from aqueous solutions by the addition of Ag^+ were not successful: the precipitates were mixtures of AgI and $Ag_4P_2O_7$ even after prolonged annealing at temperatures to 353 K and/or after preparation of disks by compacting at 1 GPa.

The products were examined by differential scanning calorimetry (DSC) using a DuPont 990 thermal analyzer. X-Ray powder patterns were obtained at room temperature in a Guinier–deWolff camera and above room temperature in a Guinier–Lenne camera. The finely divided yellow powders were stored in the dark to avoid blackening upon exposure to light.

Conductivity measurements were made by pressing polycrystalline compacts in steel dies of 5.0 or 12.5 mm diameter. The sample thicknesses varied between 1 and 5 mm, and contacts were made by adding a mixture of 50% Ag powder/50% electrolyte to the die before and after introducing the powder. The contacts and the powder were then compressed in one operation and final contact was made to the measuring electrode with conducting silver paint. The measured conductivity for a given composition increased with pelletizing pressure and for most conductivity measurements a pressure of 200 MPa was employed.

(*b*) *Single crystals of* $12AgI \cdot Ag_4P_2O_7$ ($Ag_{16}I_{12}P_2O_7$). Single crystals of $Ag_{16}I_{12}P_2O_7$ were obtained from Garrett *et al.* (*8*). Full details of the preparation are given in (*8*). The crystals were grown using a Bridgman technique by cooling a melt containing 15.5 mole% $Ag_4P_2O_7$ from 553 to 423 K at a rate of 0.5 K/hr. The quartz crucible had a conical tip and the material which formed at the tip showed striations and a distinct cleavage plane. Observations with a polarizing microscope showed uniaxial symmetry normal to the cleavage plane and such observations were employed for selecting and orienting crystals for electrical measurements parallel and perpendicular to the *c* axis. Other regions of the boule showed evidence of a vitreous phase, and while crystals in which the glassy phase was not evident were chosen, its existence could not be discounted. It was clear from both powder diffraction patterns and the high degree of optical activity that the specimens consisted at minimum of many highly oriented crystals of $Ag_{16}I_{12}P_2O_7$. However, samples softened at 353 K, about 100 K below the eutectic temperature in the equilibrium phase diagram (see below), raising the possibility that the crystallites were closely spaced in a glassy matrix. This will be discussed further in conjunction with the interpretation of the electrical data.

Conductivity measurements were made by cleavage samples to provide measurements parallel and perpendicular to the *c* axis. The faces were polished with fine sandpaper and gold contacts were made by vacuum deposition. The crystal size was on the order of 2 × 3 mm in area and 2 mm thick and the small size and complex shapes gave an uncertainty in the absolute value of the conductivity of about 30%.

(*c*) *Vitreous specimens.* A small number of vitreous specimens were prepared by quenching the melt in liquid nitrogen and by splat cooling between copper blocks actuated by optical detection of the melt falling between the blocks. Both the nitrogen-cooled glasses and the splat-cooled material showed evidence of AgI as a precipitated phase. DSC on the glasses above room temperature showed that the materials were not in equilibrium and that reactions continued above 250 K. Specimens for conductivity measurements were prepared by grinding the glasses to a fine powder and preparing a pressed compact.

2.2. *Electrical Measurements*

These measurements had to take account of potential sample polarization and the effects of contacts and the polycrystalline nature of the material. Alternating current techniques were used to prevent sample polarization, with the ac voltage being applied to the sample via a buffer amplifier with a dc output level of less than 5 mV. For the polycrystalline compacts the silver/silver electrolyte contacts showed little frequency dependence of conductivity for frequencies greater than 500 Hz over the temperature range 150–350 K. All measurements on compressed powder samples were therefore made at 1 kHz, and there was good agreement between results at this frequency and a separate experiment using a transient four-probe dc technique. A voltage proportional to the in-phase and out-of-phase components of current was detected using an Ithaco Model 393 lock-in amplifier, and standard expressions were used to calculate the equivalent parallel resistance and capacitance. At low temperatures (77 to 150 K) a General Radio 1615A capacitance bridge in a three-terminal configuration was used to measure capacitance and conductance over the frequency range 50 Hz to 50 kHz. These two measurements gave consistent results over the temperature range where the techniques overlapped.

The gold blocking electrodes used for single crystals and glasses gave an inherent frequency dependence to the measured re-

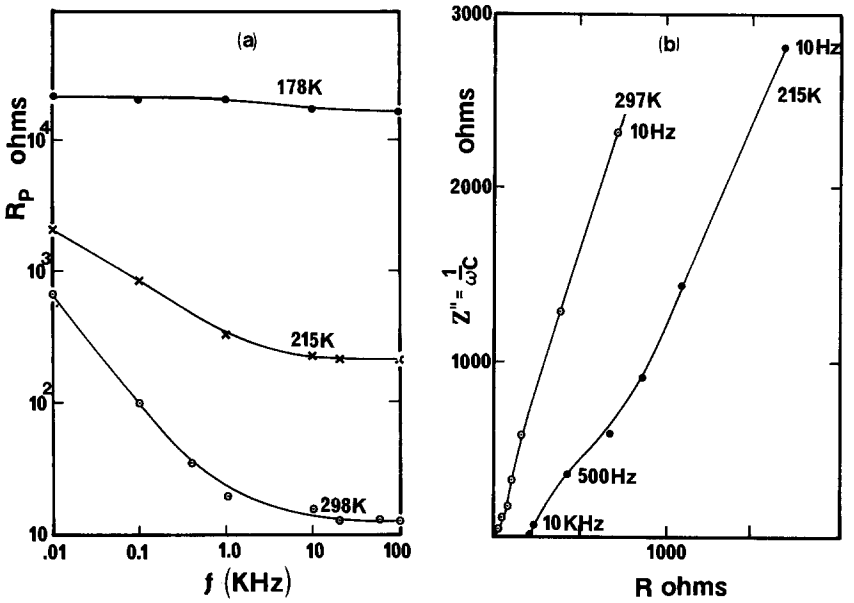

FIG. 1. Electrical characteristics of polycrystalline compacts as a function of frequency. (a) Pellet resistance. (b) Complex impedance diagram.

sistance of the sample. This was evaluated by measurements over a range of frequencies. The frequency dependence of the real part of the conductivity at different temperatures is shown in Fig. 1a and a complex plane plot of the real and imaginary parts of the conductivity is shown in Fig. 1b. At high temperatures and low frequencies a response characteristic of the electrodes was observed, while at higher frequencies (~100 kHz) the conductivity was characteristic of the bulk over all frequencies. On the basis of these results measurements of the temperature dependence of the conductivity of single crystals at high temperatures were made at a frequency of 90 kHz. At low temperatures measurements were again made using the GR 1615 bridge.

3. Results

3.1. Phase Equilibria and Crystal Structures

The starting materials, AgI and $Ag_4P_2O_7$, gave X-ray diffraction patterns in excellent agreement with those recorded in the literature (*11*). The polymorphic transitions at 423 K in AgI and at 658 K in $Ag_4P_2O_7$ were observed by DSC; the former was also observed in the Guinier–Lenne camera.

Crystalline phases are slow to form in the $AgI/Ag_4P_2O_7$ system. Rates of reaction between the iodide and phosphate below 373 K are negligible, although glasses are formed at temperatures as low as 323 K. Specimens cooled from the melt at moderate rates form glasses, particularly at phosphate concentrations between 5 and 60 mole%. However, specimens annealed at 400–430 K for 7 to 14 days and slowly cooled at room temperature gave reproducible DSC data. The phase diagram is shown in Fig. 2. The liquidus lines could not be identified with any precision by DSC and these boundaries are uncertain although they are consistent with microscopic examination of specimens quenched from temperatures of 450 to 600 K. Three compounds are formed. The first of these, $12AgI \cdot Ag_4P_2O_7$ (7.7 mole% $Ag_4P_2O_7$),

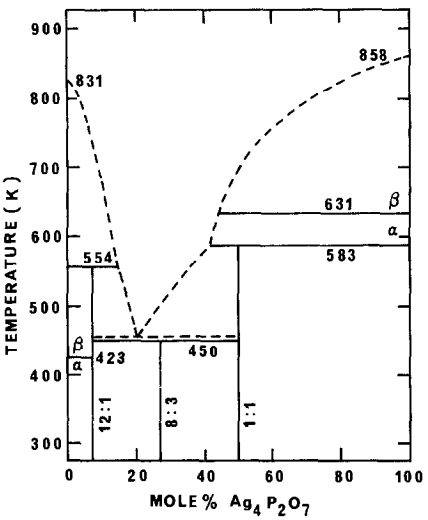

FIG. 2. Phase diagram for the AgI–$Ag_4P_2O_7$ system. Liquidus lines after Takahashi *et al.* (*2*).

melts peritectically at 554 K, forming a liquid phase and α-AgI. The second compound, $8AgI \cdot 3Ag_4P_2O_7$ (27.3 mole% $Ag_4P_2O_7$), disproportionates at 450 K to 12 $Ag_4P_2O_7$ and the third compound. The system exhibits a eutectic at almost the same temperature, the two events of disproportionation and melting being indistinguishable by DSC. The broad endothermic signal (width 9 K) which is associated with these transitions was a maximum in the range of 20–27 mole% $Ag_4P_2O_7$, but the diffraction pattern of the 8 : 3 compound was observed in room temperature specimens containing less than 20 mole% phosphate. Hence the disproportionation temperature must lie below the eutectic temperature. The third compound, $AgI \cdot Ag_4P_2O_7$ (50 mole% $Ag_4P_2O_7$), melts peritectically at 583 K, forming a liquid and α-$Ag_4P_2O_7$.

These results are at variance with the data reported by Takahashi *et al.* (*2*). In the polycrystalline powders we observed no thermal signals below 373 K, nor did we find any evidence of a cubic phase at 6.3 mole% $Ag_4P_2O_7$ corresponding to the composition $Ag_{19}I_{15}P_2O_7$. Takahashi *et al.* (*2*) stated that $Ag_{19}I_{15}P_2O_7$ dissociates into $Ag_{16}I_{12}P_2O_7$ and AgI. In our work on both polycrystalline samples and in single crystals, $Ag_{16}I_{12}P_2O_7$ could be detected free of AgI. The major difference in the two studies appears to lie in the preparative procedures; the samples in the earlier work were prepared at temperatures between 473 and 673 K (depending on composition) and free-cooled, while ours were annealed at temperatures below 450 K.

The compound $12AgI \cdot Ag_4P_2O_7$ ($Ag_{16}I_{12}P_2O_7$) is hexagonal with cell parameters a = 12.051 (1) and c = 7.497 (2) Å. These values are in good agreement with single-crystal data (*8*) and the refinement of the crystal structure requires that the composition be that stated (*8*). The structures of the 8 : 3 and 1 : 1 compounds are unknown, although the diffraction pattern of $AgI \cdot Ag_4P_2O_7$ can be indexed with reference to an orthorhombic cell with a = 9.126 (2), b = 7.795 (2), and c = 13.048 (3), Å (*11*, *12*).

3.2. Conductivity–Polycrystalline Compacts

The conductivity measured at 300 K for compositions extending across the phase diagram are shown in Fig. 3. The maximum conductivity of 0.07 ohm^{-1} cm^{-1} occurs at a composition corresponding to $12AgI \cdot Ag_4P_2O_7$ (7.7 mole%) with the conductivity–composition peak being asymmetric toward the high $Ag_4P_2O_7$ side. Minima in the conductivity were observed at compositions corresponding to the other two single-phase compositions at 27.3 and 50 mole% $Ag_4P_2O_7$, but a peak at ca. 40 mole% $Ag_4P_2O_7$ did not coincide with any feature of the phase diagram. Fig. 4 shows the temperature dependence of the conductivity of the three single-phase materials. A striking feature of the high-conductivity 12 : 1 compound is the nonlinear log σ versus $1/T$ plot which may be interpreted in terms of two activation energies, 0.14 ± 0.02 eV at high temperatures and 0.28 ± 0.02 eV at low tempera-

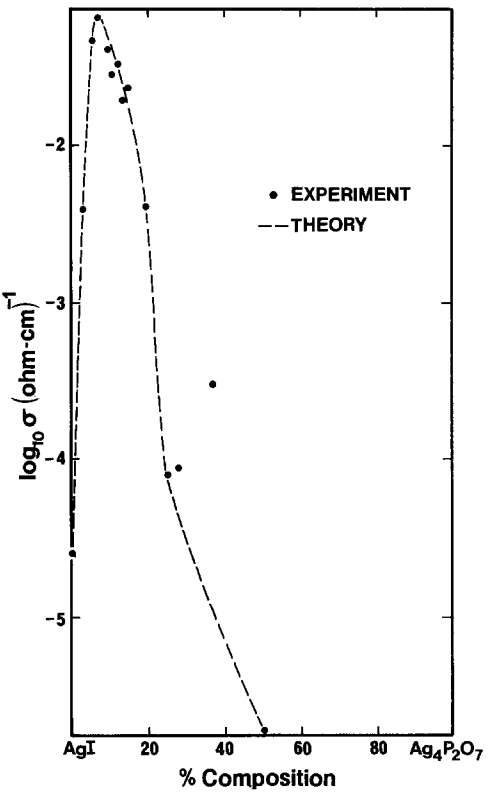

FIG. 3. Conductivity–composition diagram. Theoretical line was calculated using EMPT.

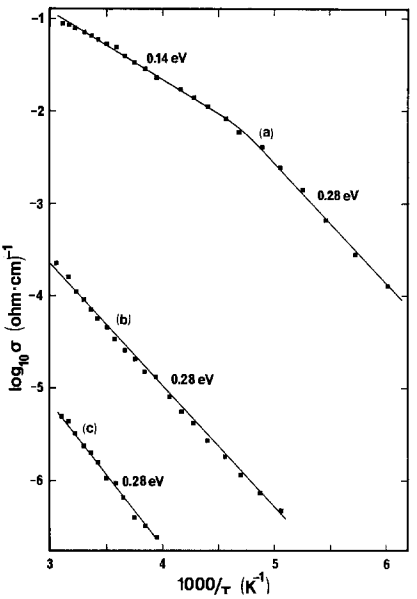

FIG. 4. Temperature dependence of conductivity for polycrystalline single-phase compounds. (a) $Ag_{16}I_{12}P_2O_7$; (b) $8AgI:3Ag_4P_2O_7$; (c) $Ag_5IP_2O_7$.

tures. The transition between the two regimes occurs at ca. 220 K. Takahashi *et al.* (*2*) reported a single activation energy of 0.14 eV, but the measurements were confined mainly to the high temperature range. Similar results have been noted in other fast-ion electrolytes, such as polycrystalline $C_5H_5NHAg_5I_6$ (*7*), $RbAg_4I_5$ (*13*), and fluorides (PbF_2 at high temperatures (*14*)), and also in vitreous $Ag_7I_4AsO_4$ (*5*). In the present work, DSC measurements showed no thermal anomalies in this temperature range indicative of a first-order phase transition or of changes in the specific heat within a measurement uncertainty on the order of 400 J (mole-K)$^{-1}$.

At low temperatures, the frequency dependence of the conductivity was more complex. Commencing as the temperature was reduced below about 150 K, the overall dielectric response showed a dispersion in both the conductivity (Fig. 5) and in the relative permittivity (Fig. 6). This dispersion occurs in a temperature range where the increasing resistivity of the bulk material is expected to outweigh the effects of grain boundaries. At the lowest temperatures, the conductivity had a frequency dependence of the form $\sigma(\omega) = A\omega^s$, where the parameter s decreased from 0.95 to 0.70 with increasing temperature (Fig. 7). The powder compact showed relatively large temperature dependence of the ac conductivity at temperatures of ~90 K. The relative permittivity increased with temperature from a high-frequency, low-temperature limit of approximately 10. This type of response is well known in electronic conductors (*15*) but a frequency dispersion characteristic of fast-ion conduction is anticipated only in the infrared (*16*). A frequency response over this temperature and frequency range has been reported in vit-

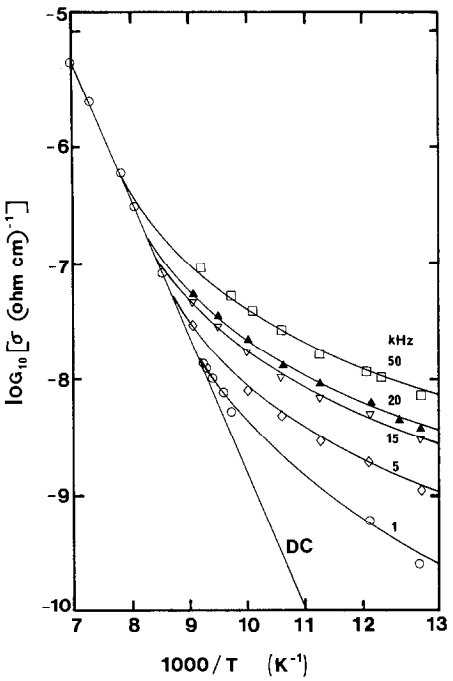

FIG. 5. Low-temperature frequency dependence of conductivity in polycrystalline $Ag_{16}I_{12}P_2O_7$.

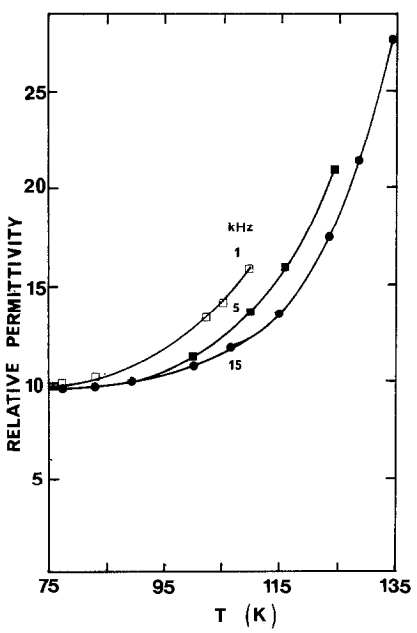

FIG. 6. Frequency and temperature of relative permittivity in polycrystalline $Ag_{16}I_{12}P_2O_7$.

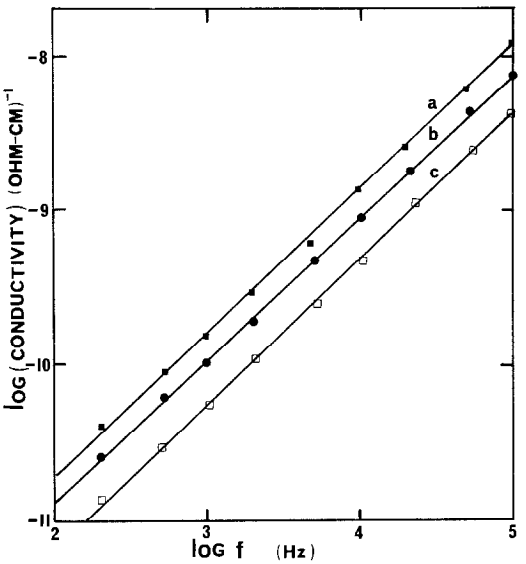

FIG. 7. Logarithmic plot of frequency dependence of conductivity at 80 K. □, Polycrystalline, $s = 0.96$, $\epsilon = 10.3$; ■, single crystal $c_{\parallel}$, $s = 0.94$, $\epsilon = 12.0$; ●, single crystal $c_{\perp}$, $s = 0.91$, $\epsilon = 13.0$.

reous silver ionic conductors (*5*) and has been attributed to some form of local ionic motion. We consider these explanations in terms of results taken on single-crystal samples.

3.3. Conductivity-Oriented Crystals of $Ag_{16}I_{12}P_2O_7$

The temperature dependence of the conductivity of a single-crystal specimen of $12AgI \cdot Ag_4P_2O_7$ oriented along the *c* axis is shown in Fig. 8. These measurements were taken using a number of measurement techniques and temperature control systems with overlapping ranges. Data for polycrystalline material of the same composition are also shown. The error bars show the uncertainty in the absolute value of the conductivity recorded in a number of specimens made from both the same and different batches of polycrystalline materials, and in different experiments on several oriented single-crystal specimens. At low temperatures (<150 K), a frequency dispersion is

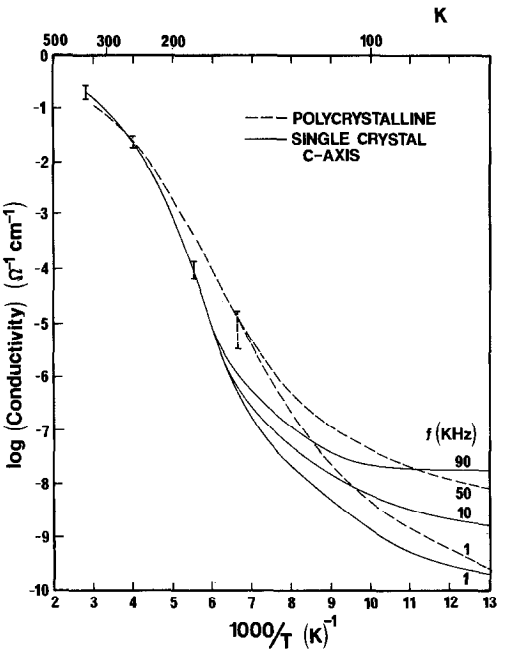

FIG. 8. Temperature dependence of conductivity at different frequencies of single-crystal $Ag_{16}I_{12}P_2O_7$ in the $c_{\parallel}$ direction and of polycrystalline $Ag_{16}I_{12}P_2O_7$. Error bars indicate range of reproducibility of material.

observed that is similar to that observed in the polycrystalline material. The principal differences lie in the absence of a temperature dependence for the conductivity at temperatures below 100 K and in the fact that the relative permittivity for the c-axis direction at 77 K is 12 ± 1.

The overall form of the results was similar for the three crystal axes (Fig. 9). Comparison of data taken on different crystals and in repeated measurements indicated that three temperature regimes could be identified. Above 200 K, no frequency dispersion was evident and measurements at 90 kHz were characteristic of the bulk material. The conductivity is anisotropic with the conductivity along the perpendicular axes being a factor of 5 or 6 times smaller than that along the c axis. The temperature dependence of the conductivity also differs along the two axes, the activation energy for conduction along the c axis changing from 0.14 eV at high temperatures to 0.4 eV at lower temperatures. This is a larger change than that observed in polycrystalline samples. This change is essentially absent along the two perpendicular axes, with the value of 0.28 eV decreasing only slightly at the highest temperature of measurement. It may also be noted that in measurements on crystals at a given temperature where the absolute value of conductivity differed from that shown, the ratio of the conductivities between the two axes was maintained.

In the temperature range 110–150 K, a frequency dispersion in the conductivity was observed with considerable variation in the temperature dependence between samples. At the lowest temperatures (77–110 K), the conductivities along the three axes were less anisotropic, although a trend whereby $\sigma_{\parallel} > \sigma_{\perp}$ remained. The frequency dependence was of the form $\sigma(\omega) = A\omega^s$, where $s > 0.9$ (Fig. 7). The low-temperature relative permittivity perpendicular to the c axis was 13 ± 1.

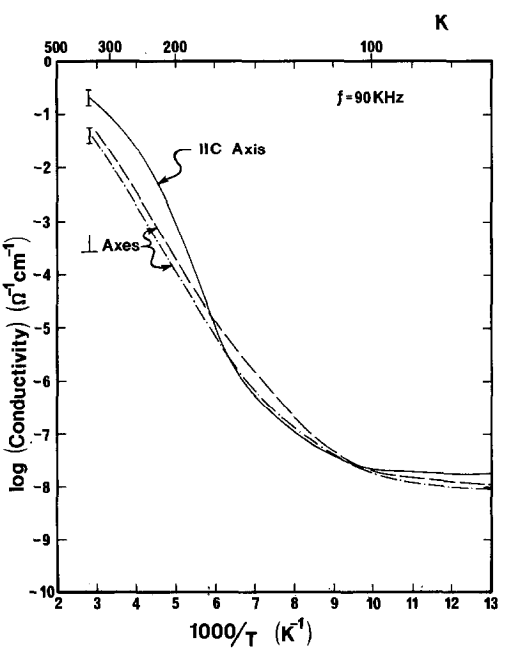

FIG. 9. Temperature dependence of bulk conductivity (90 kHz) for single crystals along $c_{\parallel}$ and two $c_{\perp}$ axes.

4. Discussion of the Experimental Data

The results of significance are the phase diagram and its correlation with the conductivity, the revised composition for the high-conductivity compound $Ag_{16}I_{12}P_2O_7$, and the ansiotropy noted in both the conductivity and the temperature dependence of the activation energy. The frequency dispersion at low temperatures is also of interest in light of similar effects observed in vitreous silver electrolytes. It is clear that results on polycrystalline compacts take some average of the properties of individual crystallites, and that the conductivity–composition diagram should reflect the phases which are present. We now examine whether such averaging effects do take place.

4.1. Prediction of the Conductivity–Composition Diagram

We consider first how effectively a mixture of two phases can account for the electrical properties. This may be done by assuming that the two phases in each phase field are intimately mixed and that the total conductivity is some form of average of the two constituent conductivities σ_1 and σ_2. For a number of disordered systems, Ast (*17*) has shown that effective medium percolation theory (EMPT) provides an appropriate average with the effective conductivity being

$$\sigma_m = 0.25\,\sigma_1\sigma_2\left\{\frac{3X_2-1}{\sigma_1}+\frac{3X_1-1}{\sigma_2}+\left[\left(\frac{3X_2-1}{\sigma_1}+\frac{3X_1-1}{\sigma_2}\right)^2+\frac{8}{\sigma_1\sigma_2}\right]^{1/2}\right\}, \quad (1)$$

where X_1 and X_2 are the volume fractions of the two components. This expression is independent of particle size and if X_1 or $X_2 = 1$ it reduces to the conductivity of an individual component. If an unknown phase of higher conductivity is present or a low conductivity arises at grain boundaries, Eq. (1) should make a poor prediction of the experimental behavior.

On the basis of the phase diagram, the measured conductivities of 0.0, 7.7, 27.3, and 50.0 mole% $Ag_4P_2O_7$ can be taken as the conductivities of the individual components. In order to determine the volume fractions we can make the approximation that the density of the four compounds are the same and calculate the molar volumes from the initial compositions. Thus in the range 0–7.7 mole% $Ag_4P_2O_7$

$$x\ AgI + y\ Ag_4P_2O_7 \rightarrow a\ AgI + b\ Ag_{16}I_{12}P_2O_7, \quad (2)$$

in the range 7.7–27.3 mole% $Ag_4P_2O_7$

$$x\ AgI + y\ Ag_4P_2O_7 \rightarrow a\ Ag_{16}I_{12}P_2O_7 + b\ 8AgI \cdot 3Ag_4P_2O_7, \quad (3)$$

and in the range 27.3–50 mole% $Ag_4P_2O_7$

$$x\ AgI + y\ Ag_4P_2O_7 \rightarrow a\ 8AgI \cdot 3Ag_4P_2O_7 + b\ Ag_5IP_2O_7. \quad (4)$$

The experimental conductivities and the conductivities calculated on the basis of Eqs. (1)–(4) are compared in Fig. 3. The agreement is good, with the asymmetry of the experimental peak being predicted by the theory. However, the composition at 40 mole% $Ag_4P_2O_7$ is anomalous. This anomaly can be interpreted from the temperature dependence of the mixed-phase systems calculated from the temperature dependence of the individual components given in Fig. 4. For a given composition, EMPT conductivities were calculated from the appropriate conductivities of the components at any given temperature. The resulting log σ versus $1/T$ plots for compositions in the high conductivity range are shown in Fig. 10a. There is agreement between experiment and theory within a factor of two over the entire temperature range. However, in the case of the 40 mole% $Ag_4P_2O_7$ composition shown in Fig. 10b, while the form of

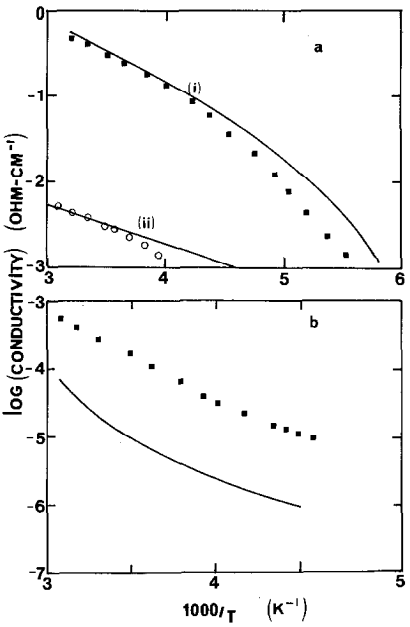

FIG. 10. Calculated and observed temperature dependences of conductivity for arbitrary compositions in the AgI–$Ag_4P_2O_7$ system. (a) (i), 11.9 mole%; (ii), 2.7 mole%. (b) Anomalous 40 mole% composition indicates resistive grain-boundary contribution.

the curve is predicted, the magnitude is lower than experiment by a factor which is constant with temperature. This suggests that a resistive third component, either due to silver migration along grain boundaries or to the presence of a vitreous phase, may have contributed to the conductivity in this phase region where the bulk conductivities of the principal components are small. In the high-conductivity regime, the correlation between the conductivity and the phase diagram suggests that the two-phase model is appropriate and that the single-phase compositions and conductivities are correct.

4.2. Anisotropic Conductivity in $Ag_{16}I_{12}P_2O_7$

We now consider whether the observed anisotropy in conductivity at high temperatures is a property of the crystal structure or is an artifact of the material. Such an artifact may arise if the crystal consists of an array of aligned crystallites in a glassy matrix of lower conductivity. The evidence for such a phase is a DSC transition at 353 K (70–80°C) observed in the crystals prepared by cooling a phosphate-rich (15.5 mole% $Ag_4P_2O_7$) melt (*8*). Such a transition was reported by Takahashi *et al.* (*2*), who prepared material in a similar fashion. No evidence for this transition was found in our polycrystalline materials which were quenched and annealed. Minami *et al.* (*6*) have noted glass transition temperatures in AgI–Ag_2O–P_2O_5 glasses between 50–70°C.

A system with aligned crystallites extending between the electrodes along the *c* axis and parallel to the electrodes in the perpendicular direction would be expected to show strong evidence of grain-boundary effects in the perpendicular direction. The ratio of conductivity along the two axes should be highly specimen dependent, and the properties of the vitreous phase should be more noticeable in the perpendicular direction. We consider these effects by examination of the frequency-dependent conductivity between 110 and 150 K. It is first necessary to establish that this conductivity is associated with the bulk dc properties and is not a function solely of electrode or intercrystalline barrier capacitances.

The ac conductivity between 110 and 150 K shows an activated behavior with an activation energy which is smaller than that observed above 200 K. The activation energy for $\sigma_\perp$ appears to be lower than that for $\sigma_\parallel$. In this region potential loss peaks due to transport of localized carriers are masked by contributions from the dc conductivity. A plot of ϵ', ϵ'', and σ versus frequency $f(\omega = 2\pi f)$ is shown in Fig. 11 for a single crystal oriented perpendicular to the *c* axis. As the frequency decreases, a continuous increase of ϵ' indicates that electrode polarization comes into play, while an increase in ϵ'' suggests a larger contribution from dc

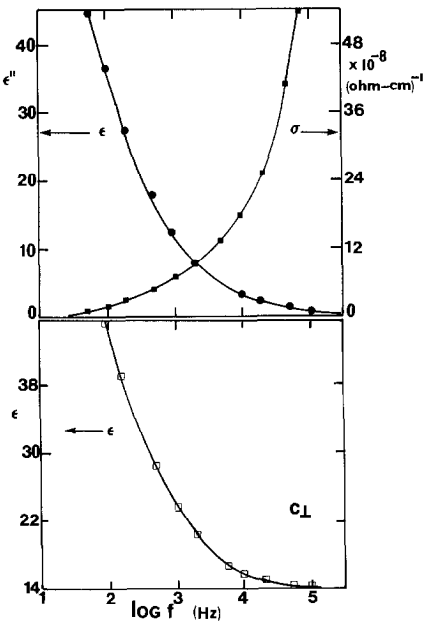

FIG. 11. Frequency dependence of dielectric parameters of single-crystal $Ag_{16}I_{12}P_2O_7$ along the $c_\perp$ direction.

conductivity. The dispersion could be attributed to a circuit model of the type shown in Fig. 12, where C_1 is the electrode capacitance, C_2 is the bulk capacitance, and R_2 is the bulk resistance. If $C_1 < C_2$ and C_1, C_2, and R_2 are independent of frequency, such a model should show at high frequencies both a conductivity and a relative permittivity which are weakly dependent on frequency. The actual behavior suggests that at least R_2 is frequency dependent and that the overall properties of the system at high frequencies are given by R_2 and C_1. Macedo *et al.* (9) have shown that electric modulus spectroscopy is useful for interpreting results on such systems. For an ideal solid electrolyte with a characteristic relaxation time ($\tau = RC = \epsilon\epsilon_0/\sigma$), the modulus of the dielectric permittivity is defined as

$$M^* = \frac{1}{\epsilon^*} = M' + jM'' = \frac{\epsilon'}{\epsilon'^2 + \epsilon''^2} + j\frac{\epsilon''}{\epsilon'^2 + \epsilon''^2}.$$

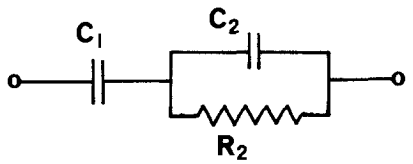

FIG. 12. Possible circuit model including barrier polarization, C_1, and bulk parameters C_2 and R_2.

A plot of M'' versus frequency f is a Debye peak with a maximum occurring when $\omega\tau = 1$.

Such a plot at fixed temperatures for a single crystal oriented perpendicular ($c_\perp$) and parallel ($c_\parallel$) to the c axis is shown in Figs. 13a and b, respectively. Well-defined peaks in M'' with a peak height and width independent of temperature are observed. At 116 K, the peak for $c_\perp$ is at 200 Hz, while that for $c_\parallel$ is at 1 kHz, consistent with the increased conductivity along $c_\parallel$ observed at higher temperatures. The difference in position of the peaks decreases with increasing frequency so that at 130 K, the peaks occur at 5 kHz for $c_\perp$ and 10 kHz for $c_\parallel$. This shows that over this temperature range, the activation energy for the relaxation time deduced from the M'' peaks is higher along the $c_\perp$ axis than along the $c_\parallel$ axis. This again is consistent with the results shown in Fig. 9.

The modulus peaks can originate from

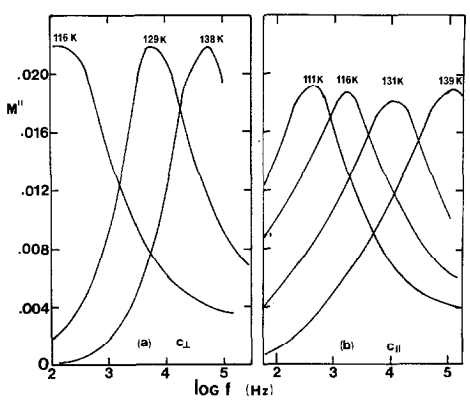

FIG. 13. Modulus M'' plot versus frequency. (a), $c_\perp$ direction; (b) $c_\parallel$ direction.

bulk effects or from intercrystalline barriers. Grant *et al.* (*5*) have shown that such peaks are broadened in poorly compressed or vitreous systems. Such effects were investigated in the present case by measurements on compressed powder compacts. Plots of M'' vs f at different temperatures for a polycrystalline sample are shown in Fig. 14. At 128 K a small peak appears around 10 kHz, which is consistent with peaks observed in crystals at this temperature. However, at lower frequencies, M'' increases, indicating a contribution of grain boundaries. At 148 K, peaks appear at 500 Hz, but M'' shows an increase again at higher frequencies. The peak at 148 K is associated with intercrystalline barriers, and the increase in M'' at higher frequencies is due to the bulk relaxation which, from Fig. 13, would be expected to occur above 10^5 Hz at 148 K. Thus the presence of intercrystalline barriers is clearly indicated by a complex form to the modulus peak, and the clear peaks in M'' for both $c_\perp$ and $c_\parallel$ in single crystals with no features above or below the relaxation frequencies indicate that along both axes the relaxation is a bulk effect. For a simple conductivity relaxation associated with the dc conductivity one would not have expected a variation of σ and ϵ'' with frequency, especially in a frequency range where peaks in M'' occur. However, Fig. 12 shows that this is clearly the case. Macedo *et al.* (*9*) have shown that this situation can arise only when there is a distribution of relaxation times τ_c. Such a distribution may arise from a distribution of activation energies within the system, although in making this postulate it is not clear whether the effects are due to polarization induced by the lack of long-range diffusion across a large potential barrier giving rise to a dipolar relaxation or to a conductivity relaxation associated with the dc conductivity. Such dipolar relaxations in vitreous systems have been explained by qualitative models suggested by Stevels (*18*) which predict slightly higher activation energies for dielectric relaxation processes, or a model suggested by Mansingh *et al.* (*19*) which predicts the same activation energy for dielectric relaxation and dc conductivity. In the present case, dipolar models may account for the greater variability between single crystals and polycrystalline samples observed between 110 and 150°C compared to other temperature ranges.

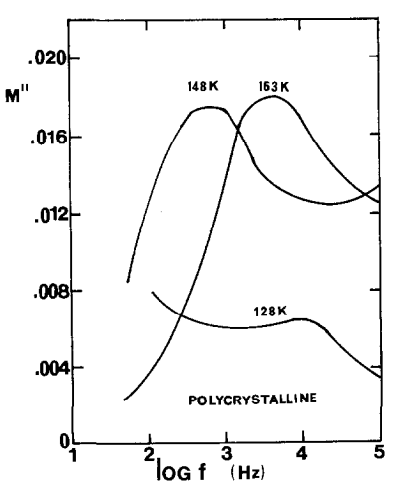

FIG. 14. Modulus M'' plot versus frequency.

The ac conductivity can be explained by two equivalent sites for an ion separated by a potential barrier $W \gg kT$. In the absence of a field the probability of occupancy is the same for both the sites, but this changes when the field is applied. The charge carriers can then either tunnel when the site energies are brought into equivalence by a suitable phonon, or hop over the barrier when the ions have sufficient thermal energy. A large distribution of jump distances for tunneling and barrier heights for hopping can give rise to a distribution of relaxation times. At temperatures below 100 K, where $\sigma = A\omega^s$, tunneling due to either ions or electrons dominates. Gough *et al.* (*20*) has suggested that the origin is electronic, while models for ionic tunneling in supe-

rionic conductors up to 40 K have been proposed (*21*). However, at such low conductivities it is difficult to estimate the relative contribution of ionic and electronic conductivities, and a categorical statement about the nature of the conduction is difficult to make. However, some contribution of ionic conductivity is indicated from the larger value of $\sigma_{\parallel}$ compared to $\sigma_{\perp}$. This difference is greatly magnified at high temperatures where ionic conduction dominates.

In the temperature range 110 to 150 K, ions have sufficient energy to hop over the barrier, giving rise to dipolar relaxation, but the peaks are masked by an increasing contribution from long-range diffusion, giving rise to dc conductivity. Finally at temperatures above 150 K, ions have sufficient energy to cross all potential barriers so that even at frequencies of 10^5Hz, the conductivity measured equals the dc value.

Models of the kind outlined above have generally been developed for vitreous systems in which the nature of the short-range order giving rise to activation energies characteristic of a given site is difficult to assess. In the case of $Ag_{16}I_{12}P_2O_7$ direct crystallographic data are available (*8*). We now examine the implication of the crystal structure for the conductivity behavior.

5. Crystal Structure

The crystal structure of $Ag_{16}I_{12}P_2O_7$ refined by Garrett *et al.* (*8*) is very similar to that found for pyridinium silver iodide by Geller and Owens (*7*). Aspects of conduction in this system have been reviewed by Geller (*13*), and Hibma (*10*) has shown that the conductivity is anisotropic, with a change in activation energy at 220 K being accounted for by a disorder–disorder transition resulting from the redistribution of ions within the unit cell. Hibma (*10*) has measured a change in specific heat in the region of the change in the slope of the conductivity plot and has shown that interactions between ions at different sites have to be taken into account. Superficial differences with $Ag_{16}I_{12}P_2O_7$ are that the transition in activation energy occurs over a wider temperature range (200–275 K), the temperature variation of the activation energy is most prominent along the *c* axis of the crystal, and a change in specific heat is not observed within the error of measurement.

In pyridinium silver iodide the iodine atoms form a well-defined hexagonal close-packed lattice with large channels running along the *c* axis. The pyridinium ions lie along the center of the channel (*7*). Three crystallographically inequivalent sites (6*f*, 4*c*, 24*m*) exist for silver ions and face-sharing octohedra linking *f* sites exist along the *c* axis. At low temperature the 6*f* and 4*c* sites are fully occupied, but at higher temperatures excitation of ions to *m* sites generates vacancies in the *f* and *c* positions, leading to rapid silver ion migration involving *f-f*, *f-m-m-f*, *c-m-m-c*, etc., pathways. Hibma (*10*) estimates the barrier between neighboring *c* sites to be 0.1 eV and between *c* or *f* sites and *m* sites to be 0.3 eV.

In $Ag_{16}I_{12}P_2O_7$, only room-temperature data are available so we can only speculate about site occupancies as a function of temperature. However, Garrett *et al.* (*8*) show a hexagonal close-packed lattice with large channels containing disordered $P_2O_7^{4-}$ ions running along the *c* axis. In this case, four sites for silver ions exist: *l*, *m*1, *m*2, *f* in two clusters (*f*, *m*1 and *l*, *m*2). Face-sharing polyhedra connect all sites within the crystal, although the major linkages lie between *f* and *m*1 and *l* and *m*2. At room temperature, the observed site occupancies are 0.52, 0.12, 0.26, and 0.29 for *f*, *m*1, *l*, and *m*2 sites, respectively. The occupancies are partly determined by the assumption that no two sites closer than the diameter of Ag^+ (2.7 Å) can be occupied, and also by the

orientation of a specific P_2O_7 ion within the *c*-axis channel.

While a final answer must await a further crystal refinement at low temperatures, the larger number of sites in $Ag_{16}I_{12}P_2O_7$ for Ag^+ may lead to a smaller change in specific heat observable in any redistribution of site occupancy compared with pyridinium silver iodide. It may be noted that from a general examination of the structure, while no direct channels exist along the *c* axis, the electrical results can be understood if conduction occurs most easily via *l* and *m*2 sites, and particularly if a temperature-dependent interaction with the disordered arrangement of $P_2O_7^{4-}$ within the adjacent channel partly determines site occupancies. The requirements outlined above for the observation of a frequency dispersion in both the ac conductivity and the relative permittivity of sites separated by different barrier heights is clearly established from crystallographic data. This is predominantly an effect of short-range order, and its observation in this system should assist in the formulation of models for vitreous systems where the order is less well defined.

6. Summary and Conclusions

The composition and electrical data presented in this paper and in the associated paper on crystal structure (*8*) have:

1. Established the equilibrium-phase diagram for the $AgI/Ag_4P_2O_7$ system. It is suggested that earlier, more complex diagrams result from the presence of nonequilibrium phases.

2. Confirmed the composition data by demonstrating that with suitable averaging procedures, a system containing only two phases can account for both the composition and temperature dependence of conductivity. In particular it is established that the composition of the phase with the highest conductivity corresponds to $Ag_{16}I_{12}P_2O_7$ rather than $Ag_{19}I_{15}P_2O_7$.

3. Shown that both the magnitude and the temperature dependence of the bulk conductivity are anisotropic and that this can be related to the occupancy of Ag^+ ion sites in the lattice and to probable interactions which occur with $P_2O_7^{4-}$ ions. Further crystallographic studies are suggested to confirm this model.

4. Shown that a frequency dispersion in the low-temperature dielectric response is a bulk property of the material related to the existence of ion sites separated by different potential barriers.

The crystal structure of $Ag_{16}I_{12}P_2O_7$ leads to many interconnected polyhedra, allowing Ag^+ ion migration through a three-dimensional network. This leads to a useful stability in the electrical properties of the material, and is the obvious reason for its technical success as a vacuum-deposited film (*3*, *4*).

Acknowledgments

The work was supported by the Natural Science and Engineering Research Council of Canada. Thanks are due to Dr. M. R. Arora and Unican Electrochemical Ltd., Montreal, for the provision of the initial powder samples. Cooperation with Dr. J. Greedan and I. D. Brown in the area of crystal growth and X-ray diffraction studies and technical assistance from J. Guillet are appreciated.

References

1. H. L. Tuller, D. P. Button, and D. R. Uhlmann, *J. Non-Cryst. Solids* **40,** 93 (1980).
2. T. Takahashi, S. Ikeda, and O. Yamamoto, *J. Electrochem. Soc.* **119,** 477 (1972).
3. M. R. Arora and J. Childs, *J. Electrochem. Soc.* **123,** 222 (1976).
4. M. R. Arora, *Thin Solid Films* **71,** 255 (1980).
5. R. J. Grant, M. D. Ingram, L. D. S. Turner, and C. A. Vincent, *J. Phys. Chem.* **82,** 2838 (1978).
6. T. Minami, Y. Takuma, and M. Tanaka, *J. Electrochem. Soc.* **124,** 1659 (1977).
7. S. Geller and B. B. Owens, *J. Phys. Chem. Solids* **33,** 1241 (1972).
8. J. D. Garrett, J. E. Greedan, R. Faggiani, S.

CARBOTTE, AND I. D. BROWN, *J. Solid State Chem.* **42,** 183 (1982).
9. P. B. MACEDO, C. T. MOYNIHAN, AND R. BOSE, *Phys. Chem. Glasses* **13,** 171 (1972).
10. T. HIBMA, *Phys. Rev. B* **15,** 5797 (1977).
11. Powder Diffraction File, JCPDS International Centre for Diffraction Data, Swarthmore, Pa., Cards 9-374, 11-637.
12. All three X-ray patterns have been submitted to the powder diffraction file (see Ref. (*11*)).
13. S. GELLER, *Phys. Rev. B* **14,** 4345 (1976).
14. C. E. DERRINGTON, A. NAVROTSKY, AND M. O'KEEFE, *Solid State Commun.* **18,** 47 (1976).
15. M. SAYER AND A. MANSINGH, *Phys. Rev. B* **6,** 4629 (1972).
16. P. BRUESCH, S. STRASSLER, AND H. R. ZELLER, *Phys. Status. Solidi A* **31,** 217 (1975).
17. D. G. AST, *Phys. Rev. Lett.* **33,** 1042 (1974).
18. J. M. STEVELS, "Encyclopaedia of Physics," Springer-Verlag, Berlin.
19. A. MANSINGH, M. SAYER, AND J. B. WEBB, *J. Non-Cryst. Solids* **28,** 123 (1978).
20. E. GOUGH, J. O. ISARD, AND J. A. TOPPING, *Phys. Chem. Glasses* **10,** 89 (1969).
21. P. J. ANTHONY AND A. C. ANDERSON, *Phys. Rev. B* **19,** 5130 (1979).